Journal of Materials Chemistry B

Accepted Manuscript

ROYAL SOCIETY OF CHEMISTRY

www.rsc.org/materialsB

Journal Name

RSCPublishing

ARTICLE

Functional Gold Nanoparticles for the Storage and Controlled Release of Nitric Oxide: Applications in Biofilm Dispersal and Intracellular Delivery

Cite this: DOI: 10.1039/x0xx00000x

Received ooth January 2012,
Accepted ooth January 2012

DOI: 10.1039/x0xx00000x

www.rsc.org/

Hien T.T. Duong,[1‡] Nik Nik M. Adnan,[2‡] Nicolas Barraud,[4‡] Johan S. Basuki,[1] Samuel K. Kutty,[3] Kenward Jung,[2] Naresh Kumar,[3] Thomas P Davis,[5*] and Cyrille Boyer[1-2*]

Abstract: Gold nanoparticles (size 10 nm) were designed to store and release nitric oxide (NO), by functionalizing their surfaces with functional polymers modified with NO-donor molecules. Firstly, block copolymer chains consisting of poly(oligoethylene glycol methyl ether methacrylate)-b-poly(vinyl benzyl chloride) (P(OEGMA)-b-PVBC)) were prepared using RAFT polymerization. The chloro- functional groups were then reacted with hexylamine, to introduce secondary amine groups to the copolymer chains. The block copolymers were then grafted onto the surface of gold nanoparticles, exploiting the end-group affinity for gold – attaining grafting densities of 0.6 chain/nm2. The secondary amine functional groups were then converted to N-diazeniumdiolate NO donor molecules via exposure to NO gas at high pressure (5 atm). The NO-bearing, gold nanoparticles were characterized using a range of techniques, including transmission electron microscopy, dynamic light scattering (DLS), thermal gravimetric analysis (TGA), and X-ray photoelectron spectroscopy (XPS). The nanoparticles displayed slow release of the nitric oxide in biological media. Proof of potential utility was then demonstrated in two different application areas: Pseudomonas aeruginosa biofilm dispersal and cancer cell cytotoxicity.

Introduction

Nitric oxide (NO) is an important biological signal molecule, being involved in the regulation of numerous physiological and pathophysiological processes such as neuronal communication, blood vessel modulation and immune response.[1,2] A decrease in endogenous production of NO due to aging, inactivity, smoking, and poor diet has been associated with many serious medical problems such as hypertension, diabetes, liver fibrosis, cardiovascular illness, neurodegenerative diseases and several cancers.[1,3-6] In addition, NO was identified as a key regulator of biofilm dispersal.[7,8] The exogenous delivery of NO to biological systems in a controlled manner is potentially desirable, but is challenging as NO gas has limited solubility in water (2-3 mM). It is extremely reactive with a short half-life of 0.1-5 seconds.[1] To overcome the problems associated with NO delivery, NO donor molecules capable of releasing NO under stimulus have been synthesized. Such donor molecules have generated a lot of research interest due to their many potential therapeutic applications. However, NO donor molecules themselves can be quite unstable,[1] for instance, NONOate (such spermine NONOate) compounds have a half-life of just a few minutes at 25°C in water.[1]

Delivery of NO from nano-encapsulated donors has become an area of increasing interest and many different nanoparticles may be applicable for NO delivery.[9] In previous work, diazeniumdiolate NO donors have been successfully conjugated to polymeric chains, e.g. ethylene/vinylacetate,[10] star polymers[11] and micelles[12]. Our group has recently reported a simple method for preparing NO-releasing polymeric micelles, with enhanced GSNO stability in aqueous media and applied the NO-nanoparticles together with cisplatin to kill neuroblastoma cancer cells.[13]

Despite the popularity of gold nanoparticles (AuNPs) only a limited number of studies have been reported for their use in nitric oxide delivery applications.[14] Schoenfisch and co-

workers have reported the grafting of water-soluble *N*-diazeniumdiolate NO donors onto AuNPs.[15,16] AuNPs are biocompatible and employed for a large range of biomedical applications, such as drug nanocarriers, computer tomography contrast agent (CT) and nanosensors.[17,18] In addition, it is possible to exploit their Plasmon resonance band for photothermal therapy, which offers an interesting way to specifically release therapeutic compounds under specific external stimuli (such light).[18] Here, we report the grafting of *N*-diazeniumdiolate conjugated macromolecules onto AuNPs yielding low-biofouling, stable NO-AuNPs and tested their ability to release NO in applications such as biofilm dispersal and cancer cell cytotoxicity studies.

Experimental Section

Materials

Oligo(ethylene glycol) methyl ether methacrylate (300 g mol^{-1}, OEGMA), 4-vinylbenzyl chloride (152.62 g mol^{-1}, 90%, VBC), gold (III) chloride trihydrate ($HAuCl_4.3H_2O$, >99%) and trisodium citrate dehydrate (>99%) were purchased from Sigma-Aldrich and used as received. 4-cyanopentanoic acid dithiobenzoate (260 g mol^{-1}, CPADB) was prepared according to Mistsukami and co-workers method.[19] 2,2'-azobisisobutylronitrile (162 g mol^{-1}, AIBN) was purchased from Sigma-Aldrich, crystallized from methanol and stored at 0°C before use. Acetonitrile, *n*-hexylamine, diethyl ether, methanol, petroleum spirit, triethylamine and toluene were used without further purification. Deuterated solvents, $CDCl_3$-*d* and DMSO-d_6 were obtained from Cambridge Isotope Laboratories, Inc. High purity N_2 (Linde gases) was used for degassing. Ultrapure deionized water (17.8 mΩ cm) was obtained using a MilliQ purification system.

Instrumental analysis

^{1}H-NMR Spectroscopy

Monomer conversions and polymer compositions were analyzed by ^{1}H-NMR using a Bruker AC300F (300 MHz) spectrometer and a Bruker DPX300 (300 MHz) spectrometer.

OEGMA monomer conversion was determined *via* ^{1}H-NMR spectroscopy by the following equation: $\alpha^{OEGMA} = 1 - (\int_{5.6\ ppm}/(\int_{4.1\ ppm}/2))$, where $\int$ is the peak integral of monomer (vinyl proton at 5.6 ppm, 1H) and the polymer (ester proton at 4.1 ppm, 2H).

The experimental $M_{n,\ NMR}$ was calculated by using the dithiobenzoate end group peak at 7.8 ppm) in the ^{1}H-NMR as a reference, as follows:

$M_{n,\ NMR} = (\int_{4.1\ ppm}/2)/(\int_{7.8\ ppm}) \times M_{W,\ OEGA} + M_{W,\ CPADB}$. $\int_{4.1\ ppm}$ and $\int_{7.8\ ppm}$ represent the peak integral of OEGMA peak at 4.1 ppm (2H) and the dithiobenzoate peak (1H) at 7.8 ppm, respectively. $M_{W,\ OEGMA}$ and $M_{W,\ CPADB}$ represent the molar mass of OEGMA CPADB, respectively.

VBC monomer conversion was determined *via* ^{1}H-NMR spectroscopy by the following equation: $\alpha^{VBC} = 1 - (\int_{5.7\ ppm}/(\int_{4.7\ ppm}/2))$, where $\int$ is the peak integral of monomer (vinyl proton at 5.7 ppm, 1H) and the polymer (benzylic proton at 4.7 ppm, 2H).

The experimental $M_{n,\ NMR}$ was calculated as follows:

$M_{n,\ NMR} = M_{n,\ NMR}^{P(OEGMA)} + (\int_{4.7\ ppm}/2)/(\int_{7.8\ ppm}) \times M_{W,\ VBC}$. $\int_{4.1\ ppm}$ and $\int_{4.7\ ppm}$ represent the integral of OEGA peak at 4.1 ppm and VBC peak at 4.7 ppm, respectively. $M_{W,\ VBC}$ and $M_{n,\ NMR}^{P(OEGMA)}$ represent the molar mass of VBC and the P(OEGMA) macroRAFT, respectively.

Size Exclusion Chromatography (SEC)

SEC analyses of polymer samples were performed in *N,N'*-dimethylacetamide [DMAc with 0.03% w/v LiBr and 0.05% 2,6-di-butyl-4-methylphenol (BHT)] at 50°C, flow rate of 1 mL min^{-1}) with a Shimadzu modular system comprising and SIL-10AD automatic injector, a Polymer Laboratories 5.0 µL bead-size guard column (50 x 7.8 mm) followed by four linear PL (Styragel) columns (105, 104, 103 and 500 Å) and an RID-10A differential refractive-index detector. The GPC calibration was performed with narrow-polydispersity polystyrene standards ranging between 104 and 2 ×000 000 g mol^{-1}. Polymer solutions at 2-3 mg mL^{-1} were prepared in the eluent and filtered through 0.45 µm filters prior to injection.

Attenuated Total Reflectance-Fourier Transform Infrared Spectroscopy (ATR-FTIR)

ATR-FTIR measurement of samples was performed using a Bruker IFS66/S Fourier transform spectrometer by averaging 128 scans with a resolution of 4 cm^{-1}. The polymer/gold hybrid nanoparticles sample was pre-dried as a thin film for ATR-FTIR analysis.

Dynamic Light Scattering (DLS) and Zeta Potential

DLS and Zeta potential measurements were performed using a Malvern Zetasizer Nano Series running DTS software (4 mW, He-Ne laser, λ = 633 nm) and an avalanche photodiode (APD) detector. The scattered light was measured at an angle of 173° for DLS measurements and at 12.8° for zeta potential measurements. The temperature was stabilized to ±0.1°C of the set temperature. All samples were prepared in MilliQ water at the concentration of ~0.2 mg/mL AuNP and filtered through a 0.45 µm pore size filter to remove dust prior to measurement. Hydrodynamic radii were calculated by the non-negative least squares (NNLS) algorithm and the zeta potential was determined by Smoluchowski approximation using manufacturer's software.

UV-Visible Spectroscopy

UV-Vis spectra were recorded in a quartz cuvette using a CARY 3000 spectrometer from Bruker at 25°C.

Transmission Electron Microscopy (TEM)

Nanoparticles size and morphologies were measured and analyzed using a JEOL 1400 transmission electron microscope at an accelerating voltage of 80 kV. A drop of samples solution was deposited onto a Formwar-coated copper grid and the water was evaporated under air. No staining was applied.

Thermal Gravimetric Analysis (TGA)

Thermogravimetric analysis (TGA) of gold nanoparticles samples were performed on a Perkin-Elmer Thermogravimetric Analyzer (Pyris 1 TGA). Samples were heated from room temperature to 150°C at constant rate of 20°C min^{-1} using air as the furnace gas. The temperature of 150°C was kept constant for 30 min to remove moisture from samples. Then, the

temperature returned to 25°C and heated again to 600°C at 20°C min^{-1}. Weight loss was calculated from the difference between weights recorded at 25°C and 600°C. The grafting density was estimated with the assumption that the nanoparticles are spherical using the weight loss and the specific surface area of gold nanoparticles (S_{AuNP}) according to the following equation:

$$\text{Grafting Density (nm}^{-2}) = \frac{(weight\ loss/M_{n,\ polymer}) \times N_a}{m_{AuNP} \times S_{AuNP}}$$

$M_{n,\ polymer}$ corresponds to the molecular weight of diblock copolymer determined by ^{1}H-NMR. N_a is Avogadro's number and m_{AuNP} is the mass of gold nanoparticles (AuNP) used for the TGA analysis (e.g. mass of nanoparticles = initial mass before TGA analysis – weight loss). The specific surface area of AuNPs (S_{AuNP}) was calculated from the particle size obtained by TEM following this relationship $d_{TEM} = 6/(\rho \times S_{AuNPs})$, where $\rho = 19.3$ g cm^{-3} is the density of metallic gold.

X-ray Photoelectron Spectroscopy (XPS)

A Kratos Axis ULTRA XPS incorporating a 165 mm hemispherical electron energy analyzer was used. The incident radiation was monochromatic A1 X-rays (1486.6 eV) at 225 W (15 kV, 15 ma). Survey (wide) scans were taken at analyzer pass energy of 160 eV. Survey scans were carried out over 1200-0 eV binding energy range with 1.0 eV steps and a dwell time of 100 ms. Samples were prepared by adding droplet of samples continuously onto aluminum sheet. Samples were dried prior to analyses.

Synthetic methods

Synthesis of P(OEGMA) MacroRAFT

$[OEGMA]_0$:$[CPADB]_0$:$[AIBN]_0$ = 35:1.0:0.2. $OEGMA_{300}$ (5.0 g, 1.67 × 10^{-3} mol), CPADB (0.128 g, 4.87 × 10^{-4} mol), AIBN (0.0159 g, 9.68 × 10^{-5} mol) and toluene (17 ml) were prepared in a 25 mL vial equipped with a magnetic stirrer bar. The reaction mixture was degassed with nitrogen for 30 minutes. The degassed solution was immersed in a pre-heated oil bath at 70°C for 17 h. the reaction was then placed in an ice bath for about 15 min to terminate polymerization and two aliquot were sampled for GPC and ^{1}H NMR analyses. The monomer conversion was determined by ^{1}H NMR analysis. The reaction medium was precipitated in petroleum spirit (boiling range 40 – 60 °C) and centrifuged (7000 rpm for 5 mins). The precipitation and centrifugation steps were repeated three times to remove any traces of unreacted monomer and then the reaction medium was dried in vacuum oven (40 °C) POEGMA was analyzed by ^{1}H NMR and GPC.

Synthesis of P(OEGMA)-b-P(VBC) copolymers

[P(OEGMA)]:[VBC]:[AIBN] = 1:100:0.2. P(OEGMA) (M_n = 10,000 g mol^{-1}) (1.0 g, 1 × 10^{-4} mol), VBC (1.53 g, 0.01 mol), AIBN (3.28 × 10^{-3} g, 2.0 × 10^{-5} mol) and acetonitrile (15 ml) were prepared in a 25 mL vial, equipped with a magnetic stirrer bar. The reaction mixture was degassed with nitrogen for 30 minutes. The degassed solution was immersed in a pre-heated oil bath at 70°C for 4 hours. The reaction was then placed in an ice bath for about 15 minutes to terminate the polymerization and two aliquot were collected for GPC and ^{1}H NMR analyses. VBC conversion was determined by ^{1}H NMR analysis. The reaction medium was precipitated in diethyl ether and centrifuged (7000 rpm for 5 mins). The purification process was repeated three times and the reaction medium was dried in vacuum oven (40 °C). Then ATR-FTIR analysis was performed to check the presence of chlorine functionality in the block copolymer (signal at 660 cm^{-1}). The block copolymer was analyzed by GPC and ^{1}H NMR.

Post-modification of P(OEGMA)-b-P(VBC) in the presence of n-hexylamine (HA) to yield P(OEGMA)-b-P(VBHA)

1.5 g of block copolymer and 1 mL of hexylamine were dissolved in toluene (10mL) in the presence of triethylamine (100 µL). The reaction mixture was prepared in a 25 mL vial, equipped with magnetic stirrer bar and was immersed in a pre-heated oil bath at 70°C for 24 hours. The reaction medium was precipitated in a mixture containing equal volume of diethyl ether and petroleum spirit and centrifuged (7000 rpm for 5 mins). Purification step were repeated for three times and the reaction medium was dried in vacuum oven (40°C). ^{1}H NMR and ATR-FTIR analysis was performed to confirm the disappearance of chlorine functionality and the presence of *n*-hexylamine functionality in the block copolymer. The resultant *P(OEGMA)-b-P(VBHA)* was analyzed by ^{1}H NMR.

Synthesis of citrate-stabilized gold nanoparticles (AuNP)

The glassware was washed with aqua regia solution, rinsed with Milli-Q water and oven dried prior to start reaction. An aqueous solution of $HAuCL_4$ (450 mL, 1 mM) was prepared and boiled on a hot plate with vigorous stirring. Then, aqueous solution of trisodium citrate (10 mL, 0.3 M) was added to $HAuCl_4$ solution rapidly.[20] The mixture was kept under reflux for 30 mins. As color of the solution changed from yellow to red wine, it was cooled to room temperature. The final AuNP solution contained a total Au^0 concentration of 0.22 mg mL^{-1} (1.10 mM).[21]

Synthesis of polymer/gold hybrid nanoparticles: AuNP@P(OEGMA)-b-P(VBHA)

A grafting 'onto' approach was performed for the synthesis of polymer/gold hybrid nanoparticles. P(OEGMA)-*b*-P(VBHA) (200mg) was dissolved in deionized water prior to mixing with AuNP solution. The polymer solution was added drop wise into AuNP solution, under vigorous stirring. The mixture was then stirred overnight in the absence of light. The reaction mixture was centrifuged three times to remove non-grafted polymer chains and excess citrate (14000 rpm for 1 hour). After removal of supernatant, the resultant AuNP@P(OEGMA)-*b*-P(VBHA) were redispersed in deionized water to acquire a concentration of 0.43 mg mL^{-1}.

Synthesis of AuNP@P(OEGMA)-b-P(VBHA/NO)

AuNP@P(OEGMA)-*b*-P(VBHA) (14 ml, 0.43 mg/ml) were redispersed in acetonitrile and methanol (6:1) mixture. The mixture was placed in a Parr apparatus and clamped. Then, the apparatus was purged with nitrogen three times and pressurized to 5 atm nitric oxide (NO) at 25°C for 2 days with constant stirring to facilitate the synthesis of *N*-diazeniumdiolate based NO donors (NONOate). The excess NO was then vented by purging with nitrogen gas. The resultant AuNP@P(OEGMA)-

b-P(VBHA/NO) were stored at 4°C until use. The theoretical amount of NO conjugated to the nanoparticles ($n^{NOtheo.}$) was calculated using the following equation:

$$n^{NOtheo.} = 2 \times [m^{AuNP@P(OEGMA)\text{-}b\text{-}P(VBHA)} \times weight\ loss\text{-}_{TGA} \times f^{VBC}] / M_n^{Copolymer}$$

where $m^{AuNP@P(OEGMA)\text{-}b\text{-}P(VBHA)}$, $weight\ loss\text{-}_{TGA}$, f^{VBC} and $M_n^{Copolymer}$ correspond to mass of composite (AuNP@P(OEGMA)-*b*-P(VBHA/NO)), weight loss determined by TGA (corresponding to the fraction of copolymer in AuNP@P(OEGMA)-*b*-P(VBHA/NO)), molar composition of VBC in the copolymer, and molecular weight of copolymer.

Nitric oxide (NO) release and their biological effect

Determination of NO release using Griess reagent kit

NO released from the nanoparticles at predetermined time intervals was measured by the standard Griess reagent kit (G7921), which is commonly used for nitrite determination.[22] AuNP@P(OEGMA)-*b*-P(VBHA/NO) were incubated in phosphate-buffered saline (pH 6.8) at ambient temperature and samples were withdrawn at specific period of time. As NO is released and readily oxidized to nitrite and nitrate when in contact with water, the nitrate was reduced to nitrite by using nitrate reductase. Griess reagent (100 µL) was added with 300 µL of the nitrite containing sample and 2.6 mL of water and incubated for 30 minutes at room temperature. Nitrite concentrations in the samples should fall within the linear range of the assay (approximately 1-100 µM). UV-vis absorbance of the resulting solution was determined at 548 nm and the total nitrite concentration in the sample solution was calculated from a standard curve and compared with theoretical values obtained from the number of VBC repeating units in the polymer backbone.

Biofilm inhibition study

The strain *P. aeruginosa* PAO1 was used to characterise the effects of NO gold nanoparticles on biofilm formation. Biofilms were grown as previously described[23] with some modifications. Briefly in all assays, overnight cultures in Luria Bertani medium were diluted to an OD_{600} of 0.005 in 1 mL M9 minimal medium (containing 48 mM Na_2HPO_4, 22 mM KH_2PO_4, 9 mM NaCl, 19 mM NH_4Cl, 2 mM $MgSO_4$, 20 mM glucose, 100 µM $CaCl_2$, pH 7.0) in tissue-culture treated 24-well plates (BD). Prior to incubation, the bacterial medium was inoculated with NO-releasing AuNP@P(OEGMA)-b-P(VBHA/NO) and 'backbone' control AuNP@P(OEGMA)-*b*-P(VBHA) treatments at final concentrations of 1 to 10 ppm, as indicated, whilst control wells were left untreated. Treatments were added to the wells, each from a 10 µl aliquot of a stock solution at the appropriate concentration of the compound dissolved in 10 mM NaOH and previously sterilized by passing through a 0.22 µm pore size filter. The plates were incubated at 37 °C with shaking at 180 rpm and the biofilms were allowed to grow for 6 h. After incubation, the planktonic biomass was quantified by removing the supernatant and measuring its OD_{600}. The remaining biofilm was washed once with PBS (1 mL), before adding 0.03% crystal violet stain made from a 1:10 dilution of Gram Crystal Violet (BD) in PBS. The plates were incubated on the bench for 20 min before washing the wells twice with PBS. Photographs of the stained biofilms were obtained using a digital camera. The amount of remaining crystal violet stained biofilm was quantified by adding 1 mL 100% ethanol and measuring OD_{550} of the homogenized suspension. OD measurements of control wells where no bacteria were added at the beginning of the experiment were subtracted from all values (i.e. OD_{600} = 0.03, and OD_{550} = 0.10). The data is presented as ratio of biofilm or planktonic bacteria compared to untreated control wells. Values measured for untreated control wells were typically OD_{600} = 0.12 for planktonic supernatants and OD_{550} = 0.20 for biofilm crystal violet staining. All assays included 2 replicates and were repeated in 2 independent experiments. Statistical analysis was performed using multiple t-test comparisons.

Biofilm dispersal study using confocal microscopy.

The glass samples with adhered bacterial cells prepared as described above were stained with Live/Dead *Bac*Light bacterial Viability Kits L-7007 (Molecular Probes, Inc., Eugene, OR) according to the manufacturer's protocol. 2 ml of the two components were mixed thoroughly in 1 ml of PBS. 10 ml of this solution were then trapped between the sample and the glass microscopy slide and allowed to incubate at room temperature in the dark for 15 min. The samples were observed with a Leitz Diaplan Scientific and Clinical microscope and an Olympus FV1000 Confocal Inverted Microscope, and imaged with Leica DFC 480 camera. For bacterial adhesion, images from 15 representative areas on each of triplicate samples for each surface were taken. Cells that were stained green were considered to be viable, those that stained red were considered to be dead as were those that stained both green and red.

Cell culture assays.

The human breast cancer cells MCF-7 were grown in Dulbecco's Modified Eagle's Medium: Nutrient Mix F-12 (DMEM) supplemented with 10% (v/v) Fetal Calf Serum (FCS) in a ventilated tissue culture flask T-75. The cells were incubated at 37°C in a 5% CO_2 humidified atmosphere and passaged every 2-3 days when monolayers at around 80% confluence were formed. Cell density was determined by counting the number of viable cells using a trypan blue dye (Sigma-Aldrich) exclusion test. For passaging and plating, cells were detached using 0.05% trypsin-EDTA (Invitrogen), stained using trypan blue dye, and loaded on the haemocytometer.

Cell viability assays.

The cytotoxicity of spermine NONOate, AuNPs@P(VBHA)-*b*-P(OEGMA) and AuNP@P(OEGMA)-*b*-P(VBHA/NO) was tested *in-vitro* by a standard Alamar Blue Assay. The assay is based on the ability of living cells to convert blue redox dye (resazurin) into bright red resorufin which can be read in a spectrophotometric reader. Nonviable cells rapidly lose metabolic capacity and thus do not generate a color signal. Thus, the intensity of the color is proportional to the cell viability. The cells were seeded at 2000 cells/well in 96 well tissue culture plates and incubated for 24 h. The medium was then replaced with fresh medium containing

spermineNONOate, AuNP@P(OEGMA)-*b*-P(VBHA) and AuNP@P(OEGMA)-*b*-P(VBHA/NO) over an equivalent NO concentration range of 0 – 500 µM. At 72 h post drug/nanoparticles incubation, treatments were removed and fresh media was added (100 µL) followed by the addition of Alamar Blue dye (20 µL) to each well. The cells were then incubated for 6 h. Cell viability was determined as a percentage of untreated control cells.

Results and discussion

Synthesis and characterization of nitric oxide (NO) conjugated polymer@gold nanoparticles

Nitric oxide (NO) - donor conjugated polymers were prepared by combining reversible addition fragmentation transfer (RAFT) polymerization[21,24] and post-modification of polymers.[25,26] The synthesis of block copolymer was achieved by RAFT polymerization.[27,28]

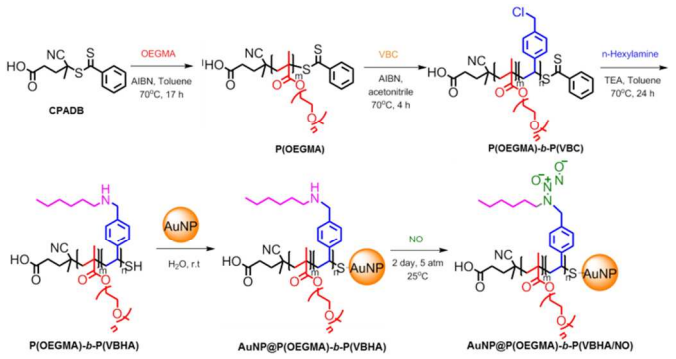

Scheme 1. Synthesis of nitric oxide (NO) conjugated polymer/gold (AuNP) hybrid nanoparticles.

Initially, polyoligo(ethylene glycol) methacrylate (P(OEGMA)) homopolymer was synthesized via RAFT polymerization using 4-cyanopentanoic acid dithiobenzoate (CPADB) as the chain transfer agent and 2,2'-azobisisobutylonitrile (AIBN) as an initiator using a molar ratio of $[OEGMA]_0$:$[CPADB]_0$:$[AIBN]_0$ = 35:1.0:0.2 (Scheme 1). The reaction was performed in toluene at 70°C for 17 h. OEGMA conversion was assessed by ^{1}H NMR and determined to be around 85%. SEC analysis confirmed the synthesis of P(OEGMA) with a low polydispersity index (PDI) of 1.16 and an average molecular weight ($M_{n,\ SEC}$) of 9,800 g/mol, in accord with the targeted molecular weight ($M_{n,\ th.}$ = 9,500 g/mol). The molecular weight of the polymer was also determined *via* ^{1}H-NMR, by utilizing the ratio of the integrals from the dithibenzoate end group at 7.8 ppm and the ester pendant groups of P(OEGMA) at 4.1 ppm (Figure 1), NMR data indicated ~32 units of OEGMA and a $M_{n,\ NMR}$ of 9,880 g/mol. After purification by precipitation in petroleum spirit (boiling range of 40-60 °C), P(OEGMA) was chain extended with 4-vinylbenzyl chloride (VBC) using a molar ratio of $[P(OEGMA)]_0$: $[VBC]_0$:$[AIBN]_0$ = 1:100:0.2. The polymerization of VBC for 4 h at 70°C in acetonitrile resulted in a 10% conversion (α) as determined by ^{1}H-NMR. The resultant block copolymer P(OEGMA)-*b*-P(VBC) was purified by precipitation in diethyl ether and subsequently analyzed by SEC, confirming a shift from low molecular weight to higher molecular weight (from 9,800 to 11,600 g/mol) and a polydispersity index of 1.2 consistent with successful chain extension (SI, Figure S1). In addition, ^{1}H-NMR confirmed the incorporation of VBC units by the presence of -CH_2Cl and aromatic signals at 4.7 ppm and 6.5-7.5 ppm, respectively (Figure 1). The molecular weight calculated by NMR ($M_{n,\ NMR}$ of 11,100 g/mol) was in accord with the SEC data (Table 1). The benzyl chloride groups from P(OEGMA)-*b*-P(VBC) were reacted with *n*-hexylamine (HA) and triethylamine at 70°C overnight, resulting in P(OEGMA)-*b*-P(VBHA). The successful modification was confirmed via ^{1}H-NMR by the emergence of new signals at 2.8 ppm and 1.3 ppm, attributed to CH_2-N and $(CH_2)_4$, respectively. The disappearance of the VBC signal at 4.7 ppm indicated complete conversion to P(OEGMA)-*b*-P(VBHA). During this transformation, the dithiobenzoate end groups were aminolyzed yielding thiol groups, as demonstrated by the disappearance of the signal at 7.8 ppm.[29,30] UV-vis was employed to confirm the absence of signal at 305 nm attributed to C=S bond after aminolysis (SI, Figure S2).

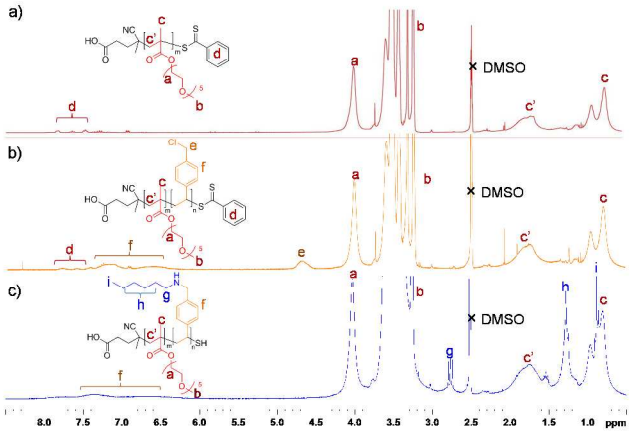

Figure 1. ^{1}H-NMR spectra of a) $P(OEGMA)_m$ (m = 32), b) $P(OEGMA)_m$-*b*-$P(VBC)_n$ (m = 32 and n = 7.3) and $P(OEGMA)_m$-*b*-$(VBHA)_n$ polymers (m = 32 and n = 7.3) (recorded in DMSO).

The thiol-terminal copolymers were grafted onto the surface of the gold nanoparticles (AuNPs), (synthesized earlier using the citric acid reduction method).[21,31] AuNPs with an average particle size of 10 nm were incubated with P(OEGMA)-*b*-P(VBHA) in water using a 33:1 w/w weight ratio of block copolymer to the AuNPs. After overnight incubation (room temperature and in the absence of light), the polymer/gold hybrid nanoparticles were purified using several centrifugation and re-dispersion cycles.[32]

The resultant AuNP@P(OEGMA)-*b*-P(VBHA) nanoparticles with secondary amine functionality were converted to diazeniumdiolate NO donors following exposure to nitric oxide (NO) gas.[33-35] AuNP@P(OEGMA)-*b*-P(VBHA) were dispersed

in a mixture of acetonitrile and methanol (6:1 v/v), purged with nitrogen for 30 min and then exposed to pressurized NO gas at 5 atm for two days at room temperature. The resultant AuNP@P(OEGMA)-b-P(VBHA/NO) were then purged with nitrogen and stored at 4°C for subsequent characterization and biological experiments.

Table 1. ^{1}H-NMR and SEC analyses of the block copolymers.

Polymer	$\alpha^{(a)}$	$M_{n,\ theor}{}^{(b)}$ (g mol^{-1})	$M_{n,\ NMR}{}^{(c)}$ (g mol^{-1})	$M_{n,\ SEC}{}^{(d)}$ (g mol^{-1})	$PDI^{(d)}$
P(OEGMA)	90%	9,700	9,900	9,800	1.16
P(OEGMA)-*b*-P(VBC)	10%	11,700	11,100	11,600	1.21
P(OEGMA)-*b*-P(VBHA)	-	-	11,800	19,600	1.60

Note: [(a)] Monomer conversion (α) was calculated by the ^{1}H-NMR of the reaction mixture by the ratio of vinyl peak at 5.6 ppm to the ester peaks at 4.1 ppm. [(b)]Theoretical molecular weight was calculated from the linear relationship $M_{n,\ theor.} = ([M]_o / [RAFT]_o) \times \alpha \times M_{w,\ monomer} + M_{w,\ RAFT}$, where $[M]_o$, $[RAFT]_o$), α, $M_{w,\ monomer}$, and $M_{w,\ RAFT}$ represent monomer and RAFT agent molar ratio, monomer conversion, molecular weight of monomer and RAFT agent, respectively. Depending on the polymerization the RAFT agent can be the CPADB or the P(OEGMA) macroRAFT. [(c)] The experimental $M_{n,\ NMR}$ was calculated by using the dithiobenzoate end group peak at 7.8 ppm ($\int_{7.8\ ppm}$) in the ^{1}H-NMR as a reference, as follows: $M_{n,\ NMR} = (\int_{4.1\ ppm}/2)/(\int_{7.8\ ppm}) \times M_{W,\ OEGMA} + (\int_{4.7\ ppm}/2)/(\int_{7.8\ ppm}) \times M_{W,\ VBC} + M_{W,\ CPADB}$. $\int_{4.1\ ppm}$ and $\int_{4.7\ ppm}$ represent the peak integral of OEGMA at 4.1 ppm and VBC peak at 4.7 ppm, respectively. $M_{W,\ OEGMA}$, $M_{W,\ VBC}$ and $M_{W,\ CPADB}$ represent the molar mass of OEGMA, VBC and CPADB, respectively. [(d)] $M_{n,\ SEC}$ and polydispersity (PDI) was measured by SEC using N,N'-dimethyl acetamide (DMAc) as eluent and polystyrene standards.

The polymer/gold hybrid nanoparticles were characterized before and after NO conjugation to afford a comparison. ATR-FTIR analysis confirmed the grafting of block copolymers onto AuNPs (SI, Figure S3) by the presence of ether (C-O) and ester (C=O) at 1100 cm^{-1} and 1730 cm^{-1}, respectively.[36] A broad absorption at around 3500 cm^{-1} was indicative of the secondary amine conjugated to the AuNP@P(OEGMA)-*b*-P(VBHA). After NO conjugation, only a minimal change to the spectrum was evident, as a slightly broad peak at around 1600 cm^{-1} appeared and was attributed to the N=O vibration.[37] X-ray photoelectron spectroscopy (XPS) confirmed NO conjugation by an increase in the signal from nitrogen (N1s) intensity at around 399.7 eV (from 0.6 to 1.5 atomic percentage) consistent with the formation of *N*-diazeniumdiolate (SI, Figure S4). The intensity of the carbon (C1s) peak decreased slightly because of the higher concentrations of nitrogen and oxygen after NO conjugation (SI, Figure S5). The increase of oxygen (O1s) intensity with the emergence of a signal at 531 eV (in addition to 533 eV), indicative of N=O functionality.[38,39] The ratio of atomic percentages of carbon (C1s) and gold (Au4f7) decreased slightly after conjugation with NO, suggesting some detachment of polymer from AuNP@P(OEGMA)-*b*-P(VBHA) during the reaction with NO. Thermal gravimetric analysis (TGA) was used to quantify the amount of polymer grafted to the AuNPs (SI, Figure S6). TGA indicated 28% weight loss corresponding to 0.68 ± 0.14 chain.nm^{-2} for 10 nm gold nanoparticles (Table 2). Following NO conjugation, we observed a slightly lower weight loss (25%) corresponding to a grafting density of 0.59 ± 0.12 chain.nm^{-2}, suggesting the detachment of some grafted polymer chains during the treatment with NO gas. The exact amount of conjugated NO could not be determined by TGA, since some nitric oxide gas was released during solvent evaporation.

P(OEGMA) grafting onto gold nanoparticles is known to imbue bio-compatibility, hydrophilicity and anti-fouling properties, promoting stability in biologically relevant media.[24] Consistent with the known propensity of PEG to stabilize AuNPs, the grafted block copolymer imparted colloidal stability to the gold nanoparticles.[20] UV-Vis absorption of AuNP@P(OEGMA)-*b*-P(VBHA) in water showed a bathochromic shift in the Plasmon absorbance band indicating a change in local refractive index (518 → 523 nm), indicative of the polymer layer and higher colloidal stability[40] (Figure 2A).

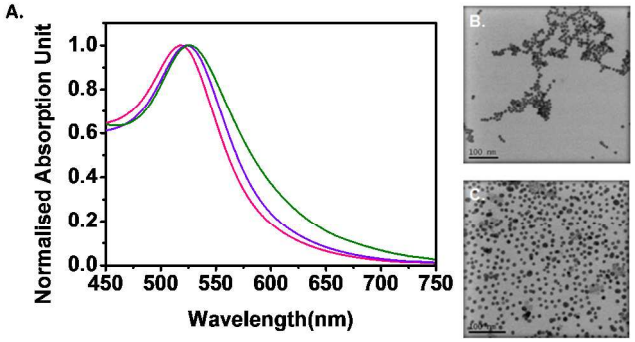

Figure 2. A) UV-Vis absorption spectra of AuNPs (pink line), AuNP@P(OEGMA)-*b*-P(VBHA) (purple line), and AuNP@P(OEGMA)-*b*-P(VBHA/NO) (green line). B) A TEM micrograph of neat gold nanoparticles (AuNP). C) A TEM micrograph of AuNP@P(OEGMA)-*b*-P(VBHA/NO).

There was no significant shift in the UV-Vis absorption following conjugation with NO, indicating that the colloidal stability of the nanoparticles was maintained. Transmission electron microscopy (TEM) confirmed the enhancement of colloidal stability in the AuNP@P(OEGMA)-*b*-P(VBHA) in comparison with the aggregating neat gold nanoparticles (Figure 2B and 2C). A uniform distribution of spherical nanoparticles with an average particle size of 10 nm was observed in the TEM, in accord with the hydrodynamic size data obtained from dynamic light scattering (DLS) measurements (Figure 3). After the NO conjugation a slight increase in hydrodynamic size was noted, attributed to hydrophilic or zwitterionic functionalities introduced by the formation of *N*-diazeniumdiolate in the hydrophobic *n*-hexylamine substituted benzyl groups. The zeta potentials (ζ) of the AuNPs were significantly altered after grafting with block copolymer.[41] An increase in zeta potential was consistent with the exchange of citric acid with the thiol terminated block copolymers, coating the AuNPs with a neutral P(OEGMA)

outer layer (Table 2). Negative zeta potentials (-13 ± 3 mV) of AuNP@P(OEGMA)-*b*-P(VBHA) was attributed to the presence of 4-cyanopentanoic acid RAFT groups on the periphery of the nanoparticles. The results from TGA, DLS and zeta potential measurements are summarized in Table 2.

Table 2. Zeta potential, DLS and TGA measurements of polymer/gold hybrid nanoparticles.

Nanoparticles	ζ[(a)] (mV)	d_{DLS}[(b)] (nm)	*Weight loss* $_{TGA}$[(c)]	*Grafting density*[(d)] (nm^{-2})
AuNPs	-55 ± 5	10 ± 5	-	-
AuNPs@P(OEGMA)-*b*-P(VBHA)	-13 ± 3	19 ± 8	28%	0.68 ±0.14
AuNPs@P(OEGMA)-*b*-P(VBHA/NO)	-15 ± 5	24 ± 9	25%	0.59 ±0.12

Note: [(a)] Zeta potential (ζ) of polymer/gold hybrid nanoparticles in deionized water.[(b)]Number-weighted particle size (d_{DLS}) or hydrodynamic size measurement in deionized water at the concentration of 0.2 mg/mL AuNP. [(c)] Weight loss in pre-dried polymer/gold hybrid nanoparticles determined by TGA. [(d)] Grafting density of block copolymer on the surface of AuNP was calculated was calculated by the following equation:
Grafting density = (weight loss-$_{TGA}$ / $M_{n,\,NMR}$)× N_a / (m_{AuNP} × S_{AuNP}), where m_{AuNP} and N_a represent the mass of gold nanoparticles and Avogadro number respectively. S_{AuNP} or specific surface area of gold nanoparticles was calculated based on 10 nm particle size of AuNP and a specific gravity of 19.3 g/cm.

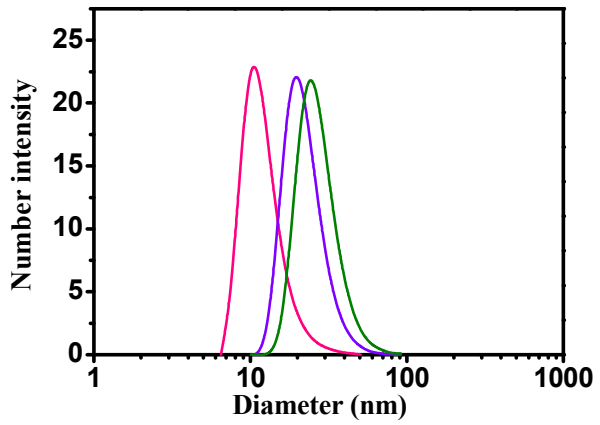

Figure 3. Hydrodynamic diameter analysis via DLS (concentration of nanoparticle solution of 1 mg.ml-1 of AuNPs (pink line), AuNP@P(OEGMA)-b-P(VBHA) (purple line), and AuNP@P(OEGMA)-b-P(VBHA/NO) (green line).

Release of NO from AuNP@P(OEGMA)-*b*-P(VBHA/NO)

The release of NO from *N*-diazeniumdiolate NO donors was performed in phosphate buffer (pH 6.8) at ambient temperature (Note: a similar release rate was observed at pH 7.0).[4,42,43] After separation of the AuNPs by centrifugation, the supernatant was analyzed using a Griess assay. Released NO was converted to nitrate and nitrite when in contact with water, followed by the reduction of nitrate to nitrite using nitrate reductase and its co-factor.[22] The subsequent addition of a Griess reagent to the nitrite sample yielded a diazonium salt that was converted instantaneously to an azo dye with a UV-Vis absorption maximum at 548 nm (SI, Figure S7). Using a calibration curve (1-100 µM), the concentration of released NO was monitored gradually over a 6 days period (Figure 4). In comparison to the small molecule *N*-diazeniumdiolate based NO donor,[4,44] the release rate of NO from AuNP@P(OEGMA)-*b*-P(VBHA/NO) was slow and there was no burst release of NO demonstrating a higher stability of NO-donor when encapsulated in the polymer/gold hybrid nanoparticles. For example, spermine NONOate (Z)-1-[N-[3-aminopropyl]-N-[4-(3-aminopropylammonio)butyl]-amino]diazen-1-ium-1,2-diolate), a fast NO donor presents a half-life time ($t_{1/2}$ = 40 min at pH 7.4, 37 ºC), while other NONOate donors with more stable NO release profiles in buffered systems (compared to spermine NONOate), such as (Z)-1-[N-(2-aminoethyl)-N-(2-ammonioethyl)amino]diazen-1-ium-1,2-diolate (DETA) or (Z)-1-[N-(3-aminopropyl)-N-(3-ammoniopropyl)amino]diazen-1-ium-1,2-diolate presents half-life time of few hous (DETA NONOate; $t_{1/2}$ = 20h and DPTA NONOate; $t_{1/2}$ = 3h at pH 7.4, 37 ºC).

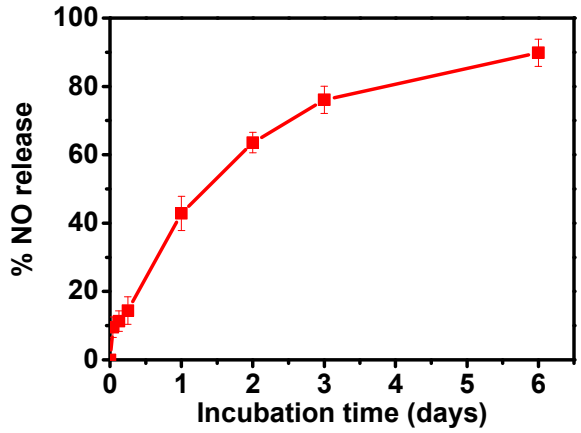

Figure 4. Study of NO release from AuNP@P(OEGMA)-*b*-P(VBHA/NO) in phosphate buffer solution (PBS) at pH 6.8 at room temperature, experiments done in triplicate.

Antibiofilm properties of AuNP@P(OEGMA)-*b*-P(VBHA)

Recently, researchers have identified that NO can trigger the biofilm dispersal.[7,8,23,45] We decided to investigate the effect of AuNP@P(OEGMA)-*b*-P(VBHA/NO) on biofilm formation in the opportunistic pathogen and model organism *Pseudomonas aeruginosa*. Biofilms were grown in minimal M9 medium in the presence of 2.5 and 10 ppm (or 0.0025 and 0.010 mg/mL) of AuNP@P(OEGMA)-*b*-P(VBHA/NO) were found to inhibit biofilm formation after 6 h compared to untreated biofilms with a 67% (P = 0.18) and 83% (P < 0.001) reduction in biofilm biomass. Treatment with AuNPs@P(VBHA/NO)-*b*-P(OEGMA) (NO concentration of 10 ppm) also induced a

decrease in planktonic growth in culture, resulting in 34% less suspended biomass after 6 h compared to untreated wells (Figure 5A). As a control experiment, AuNP@P(OEGMA)-*b*-P(VBHA) was tested at the lowest (1 ppm) and highest (10 ppm) concentrations and showed no effect on biofilm or planktonic growth in *P. aeruginosa* cultures, suggesting that the observations above are related to NO released from AuNP@P(OEGMA)-*b*-P(VBHA/NO) rather than any side effect from the nanoparticle carrier (Figure 5).

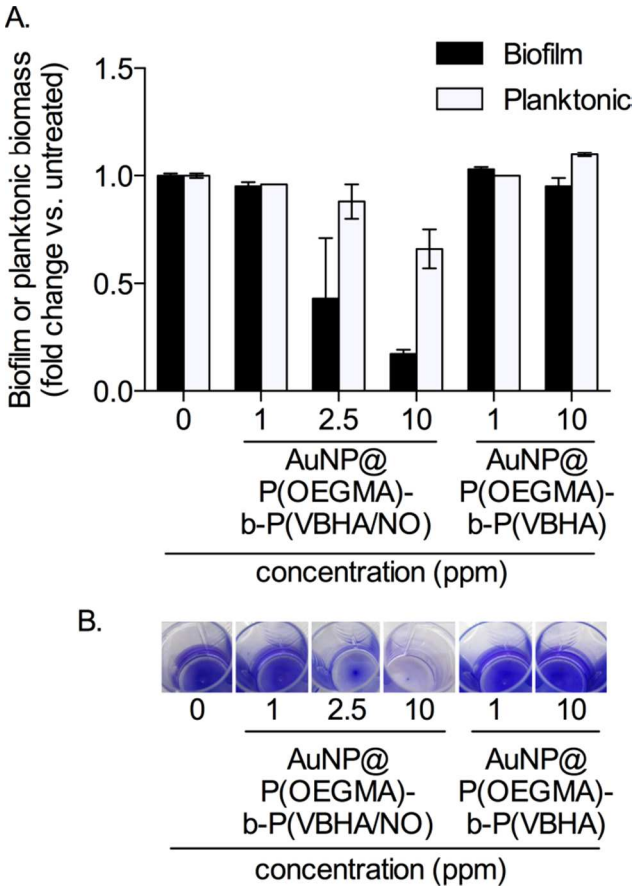

Figure 5. Dose dependent prevention of biofilm formation. (A) *P. aeruginosa* biofilms were grown for 6 h in the presence or absence of AuNP@P(OEGMA)-*b*-P(VBHA/NO) (1-10 ppm of AuNP@P(OEGMA)-*b*-P(VBHA/NO) and AuNP@P(OEGMA)-*b*-P(VBHA)) before assessing planktonic growth by measuring the OD_{600} of the supernatant and analyzing biofilm biomass by crystal violet staining. Error bars represent standard error or the means (n = 2); (B) Stained biofilms treated with the indicated concentrations of NO releasing and backbone control nanoparticles.

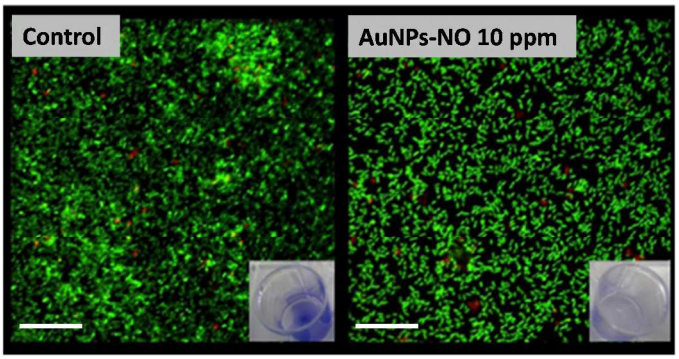

Figure 6. Biofilm dispersal study of *Pseudomonas Aureginosa* after the treatment (right) with AuNP@P(OEGMA)-*b*-P(VBHA/NO) (AuNPs-NO, concentration of 10 ppm). Under confocal microscopy green and red stains indicate viable and dead cells, respectively. Inset- The presence of biofilm was characterized by the stain of crystal violet, scale bar = 50 µm.

Confocal microscopy was used to evaluate the ability of the AuNP@P(OEGMA)-*b*-P(VBHA/NO) to prevent colonization and biofilm dispersal of *P. aeruginosa*. After treatment with AuNP@P(OEGMA)-*b*-P(VBHA/NO), there is a significant reduction in biofilm bio-volume and increased biofilm dispersal compared to the untreated control (Figure 6).

AuNP@P(OEGMA)-*b*-P(VBHA/NO) Donors against cancer

Recent publications reveal that NO can have anti-cancer properties at micromolar concentration.[46-49] Indeed, large concentrations of NO (i.e., micromolar) produce reactive nitrogen species, which along with reactive oxygen species result in oxidative and nitrosative stress, leading to DNA base deamination, nitrosylation of enzymes, impaired cellular function, inhibited mitochondrial respiration and cell apoptosis.[47]

We next tested the cytotoxicity of the nanoparticles on MCF-7 breast cancer and MRC5 cells using an Alamar Blue Assay after exposure with NO nanoparticles for 72 h. Spermine NONOate, AuNP@P(OEGMA)-*b*-P(VBHA) and AuNP@P(OEGMA)-*b*-P(VBHA/NO) were tested over an equivalent NO concentration range of 5-500 µM. As expected, the AuNP@P(OEGMA)-*b*-P(VBHA) were shown to be non-toxic at the concentration equivalent to NO concentrations up to 500 µM (viability above 80% after 3 days of incubation) (Figure 7) for both cells. AuNP@P(OEGMA)-*b*-P(VBHA/NO) was more toxic for MCF-7 breast cancer at 60 µM (~26% cell viability) than for non-cancerous cells (MRC-5, 49% cell viability). It is noted that AuNP@P(OEGMA)-*b*-P(VBHA/NO) present a greater toxicity toward MCF-7 breast cancer cells than small organic NO donor (spermine NONOate) (Figure 7).

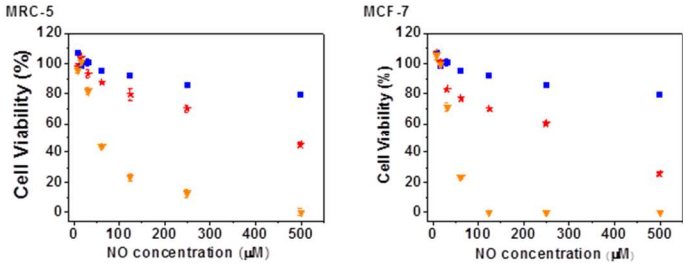

Figure 7. Toxicity of spermine NONOate (red star), AuNP@P(OEGMA)-*b*-P(VBHA) (blue square), AuNP@P(OEGMA)-*b*-P(VBHA/NO) (orange triangle) in MCF-7 breast cancer cells and MRC-5 cells, experiments done in triplicate.

Conclusions

In summary, we have developed hybrid organic/inorganic gold nanoparticles for the delivery of NO. Gold nanoparticles were functionalized with a non-biofouling polymer layer that incorporated diazeniumdiolate NO donor molecules. The NO was released slowly at pH 6.8, and the nanoparticle-delivery approach was shown to be effective in two different applications: biofilm dispersal and cancer cell cytotoxicity. The prepared gold nanoparticles illustrate the versatility of the system and the great potential for biomedical application.

Acknowledgment.

The authors thank the Nuclear Magnetic Resonance facility, Biomedical Imaging facility and the Electron Microscope Unit at the Mark Wainwright Analytical Centre for helpful discussions and advice on the design of the experimental setup. NB is supported by ARC grant DE120101604. CB is thankful for his fellowship from Australian Research Council (Future Fellowship (ARC-FT 120100096)).

Supporting information.

Experimental details, molecular weight distribution, FTIR spectra and XPS spectra (Figures S1 to S6). This material is available free of charge *via* the internet at http://pubs.acs.org.

References

[1]Australian Centre for Nanomedicine, School of Chemical Engineering, University of New South Wales, Sydney, Australia 2052
[2]Centre for Advanced Macromolecular Design (CAMD), School of Chemical Engineering, University of New South Wales, Sydney, Australia 2052
[3]School of Chemistry, University of New South Wales, Sydney, Australia 2052
[4]Centre for Marine Bio-Innovation, School of Biotechnology and Biomolecular Sciences
University of New South Wales, Sydney, Australia 2052
[5]ARC Centre of Excellence in Convergent Bio-Nano Science & Technology, Monash Institute of Pharmaceutical Sciences, Monash University, Parkville, Melbourne 3052; Department of Chemistry, University of Warwick, UK
*Corresponding authors, E-mails: cboyer@unsw.edu.au; Thomas.p.davis@monash.edu

± Equal contribution

(1) T. B. Cai; P. G. Wang; A. A. Holder *In Nitric Oxide Donors: For Pharmaceutical and Biological Applications*; Wiley-VCH: Weinheim, 2005.
(2) P. G. Wang; M. Xian; X. Tang; X. Wu; Z. Wen; T. Cai; A. J. Janczuk *Chem. Rev.* 2002, **102**, 1091-1134.
(3) A. W. Carpenter; M. H. Schoenfisch *Chem. Soc. Rev.* 2012, **41**, 3742-3752.
(4) P. N. Coneski; M. H. Schoenfisch *Chem. Soc. Rev.* 2012, **41**, 3753-3758.
(5) A. B. Roy; O. E. Petrova; K. Sauer *J. Bacteriol.* 2012, **194**, 2904-2915.
(6) N. Liu; Y. Xu; S. Hossain; N. Huang; D. Coursolle; J. A. Gralnick; E. M. Boon *Biochemistry* 2012, **51**, 2087-2099.
(7) D. McDougald; S. A. Rice; N. Barraud; P. D. Steinberg; S. Kjelleberg *Nat. Rev. Microbiol.* 2012, **10**, 39-50.
(8) N. Barraud; D. J. Hassett; S. H. Hwang; S. A. Rice; S. Kjelleberg; J. S. Webb *J. Bacteriol.* 2006, **188**, 7344-7353.
(9) D. A. Riccio; M. H. Schoenfisch *Chem. Soc. Rev.* 2012, **41**, 3731-3741.
(10) E. N. Momin; K. E. Schwab; K. L. Chaichana; R. Miller-Lotan; A. P. Levy; R. J. Tamargo *Neurosurgery* 2009, **65**, 937-945.
(11) S. F. Duan; S. Cai; Q. H. Yang; M. L. Forrest *Biomaterials* 2012, **33**, 3243-3253.
(12) Y. S. Jo; A. J. van der Vlies; J. Gantz; T. N. Thacher; S. Antonijevic; S. Cavadini; D. Demurtas; N. Stergiopulos; J. A. Hubbell *J. Am. Chem. Soc.* 2009, **131**, 14413-14418.
(13) H. T. T. Duong; Z. M. Kamarudin; R. B. Erlich; Y. Li; M. W. Jones; M. Kavallaris; C. Boyer; T. P. Davis *Chem. Commun.* 2013, **49**, 4190-4192.
(14) P. Sudhesh; K. Tamilarasan; P. Arumugam; S. Berchmans *ACS Appl. Mater. Inter.* 2013, **5**, 8263-8266.
(15) M. A. Polizzi; N. A. Stasko; M. H. Schoenfisch *Langmuir* 2007, **23**, 4938-4943.
(16) A. R. Rothrock; R. L. Donkers; M. H. Schoenfisch *J. Am. Chem. Soc.* 2005, **127**, 9362-9363.
(17) R. A. Sperling; P. Rivera Gil; F. Zhang; M. Zanella; W. J. Parak *Chem. Soc. Rev.* 2008, **37**, 1896-1908.
(18) A. Kumar; X. Zhang; X.-J. Liang *Biotech. Adv.* 2013, **31**, 593-606.
(19) Y. Mitsukami; M. S. Donovan; A. B. Lowe; C. L. McCormick *Macromolecules* 2001, **34**, 2248-2256.
(20) P. Alexandridis *Chem. Eng. Techn.* 2011, **34**, 15-28.
(21) M. Beija; Y. Li; H. T. Duong; S. Laurent; L. V. Elst; R. N. Muller; A. B. Lowe; T. P. Davis; C. Boyer *J. Mat. Chem.* 2012, **22**, 21382-21386.
(22) J. Sun; X. Zhang; M. Broderick; H. Fein *Sensors* 2003, **3**.
(23) N. R. Yepuri; N. Barraud; N. Shah Mohammadi; B. G. Kardak; S. Kjelleberg; S. A. Rice; M. J. Kelso *Chem. Commun. (Cambridge, England)* 2013, **49**, 4791-4793.
(24) C. Boyer; M. R. Whittaker; M. Luzon; T. P. Davis *Macromolecules* 2009, **42**, 6917-6926.
(25) C. Fu; B. Yang; C. Zhu; S. Wang; Y. Zhang; Y. Wei; L. Tao *Polym. Chem.* 2013, **4**, 5720-5725.
(26) B. Yang; Y. Zhao; C. Fu; C. Zhu; Y. Zhang; S. Wang; Y. Wei; L. Tao *Polym. Chem.* 2014, **5**, 2704-2708.
(27) L. Tao; J. Xu; D. Gell; T. P. Davis *Macromolecules* 2010, **43**, 3721-3727.
(28) D. J. Keddie *Chem. Soc. Rev.* 2014, **43**, 496-505.
(29) H. Willcock; R. K. O'Reilly *Polym. Chem.* 2010, **1**, 149-157.
(30) P. J. Roth; C. Boyer; A. B. Lowe; T. P. Davis *Macro. Rapid Comm.* 2011, **32**, 1123-1143.
(31) J. Polte; T. T. Ahner; F. Delissen; S. Sokolov; F. Emmerling; A. F. Thünemann; R. Kraehnert *J. Am. Chem. Soc.* 2010, **103**, 1296-1301.
(32) M. Liang; I.-C. Lin; M. R. Whittaker; R. F. Minchin; M. J. Monteiro; I. Toth *ACS Nano* 2010, **4**, 403-413.
(33) A. R. Rothrock; R. L. Donkers; M. H. Schoenfisch *J. Am. Chem. Soc.* 2005, **127**, 9362-9363.

(34) M. A. Polizzi; N. A. Stasko; M. H. Schoenfisch *Langmuir* 2007, **23**, 4938-4943.
(35) J. H. Shin; S. K. Metzger; M. H. Schoenfisch *J J. Am. Chem. Soc.* 2007, **129**, 4612-4619.
(36) J. S. Basuki; H. T. T. Duong; A. Macmillan; R. Whan; C. Boyer; T. P. Davis *Macromolecules* 2013, **46**, 7043-7054.
(37) T. E. Hoost; K. Otto; K. A. Laframboise *J. Catalysis* 1995, **155**, 303-311.
(38) X. Bao; U. Wild; M. Muhler; B. Pettinger; R. Schloegl; G. Ertl *Surface Science* 1999, **425**, 224-232.
(39) T. Herranz; X. Deng; A. Cabot; Z. Liu; M. Salmeron *J. Catalysis* 2011, **283**, 119-123.
(40) M. I. Gibson; M. Danial; H.-A. Klok *ACS Comb. Sci.* 2011, **13**, 286-297.
(41) C. Boyer; M. R. Whittaker; K. Chuah; J. Liu; T. P. Davis *Langmuir* 2010, **26**, 2721-2730.
(42) E. V. Stevens; A. W. Carpenter; J. H. Shin; J. Liu; C. J. Der; M. H. Schoenfisch *Mol. Pharmaceutics* 2010, **7**, 775-785.
(43) P. Taladriz-Blanco; V. Pastoriza-Santos; J. Pérez-Juste; P. Hervés *Langmuir* 2013, **29**, 8061-8069.
(44) D. J. Smith; D. Chakravarthy; S. Pulfer; M. L. Simmons; J. A. Hrabie; M. L. Citro; J. E. Saavedra; K. M. Davies; T. C. Hutsell; D. L. Mooradian; S. R. Hanson; L. K. Keefer *J. Med. Chem.* 1996, **39**, 1148-1156.
(45) N. Barraud; D. Schleheck; J. Klebensberger; J. S. Webb; D. J. Hassett; S. A. Rice; S. Kjelleberg *J. Bacteriol.* 2009, **191**, 7333-7342.
(46) S. Mocellin; V. Bronte; D. Nitti *Med. Res. Rev.* 2007, **27**, 317-352.
(47) D. A. Wink; Y. Vodovotz; J. Laval; F. Laval; M. W. Dewhirst; J. B. Mitchell *Carcinogenesis* 1998, **19**, 711-721.
(48) E. V. Stevens; A. W. Carpenter; J. H. Shin; J. Liu; C. J. Der; M. H. Schoenfisch *Mol. Pharmaceutics* 2010, **7**, 775-785.
(49) V. Kumar; S. Y. Hong; A. E. Maciag; J. E. Saavedra; D. H. Adamson; R. K. Prud'homme; L. K. Keefer; H. Chakrapani *Mol. Pharmaceutics* 2009, **7**, 291-298.

Journal Name

RSCPublishing

ARTICLE

Functional Gold Nanoparticles for the Storage and Controlled Release of Nitric Oxide: Applications in Biofilm Dispersal and Intracellular Delivery

Hien T.T. Duong,[1±] Nik Nik M. Adnan,[2±] Nicolas Barraud,[4±] Samuel K. Kutty,[3] Johan S. Basuki,[1] Kenward Jung,[2] Naresh Kumar,[3] Thomas P Davis,[5*] and Cyrille Boyer[1-2*]

[1]*Australian Centre for Nanomedicine, School of Chemical Engineering, University of New South Wales, Sydney, Australia 2052*

[2]*Centre for Advanced Macromolecular Design (CAMD), School of Chemical Engineering, University of New South Wales, Sydney, Australia 2052*

[3]*School of Chemistry, University of New South Wales, Sydney, Australia 2052*

[4]*Centre for Marine Bio-Innovation, School of Biotechnology and Biomolecular Sciences*

University of New South Wales, Sydney, Australia 2052

[5]*ARC Centre of Excellence in Convergent Bio-Nano Science & Technology, Monash Institute of Pharmaceutical Sciences, Monash University, Parkville, Melbourne 3052; Department of Chemistry, University of Warwick, UK*

**Corresponding authors, E-mails: cboyer@unsw.edu.au; Thomas.p.davis@monash.edu*

± Equal contribution

Graphical abstract